Atmos. Chem. Phys. Discuss., https://doi.org/10.5194/acp-2017-890
Manuscript under review for journal Atmos. Chem. Phys.
Discussion started: 1 December 2017


Atmospheric Chemistry and Physics Discussions
Open Access

# Estimations of anthropogenic dust emissions at global scale from 2007 to 2010

Siyu Chen[1], Jianping Huang[1*], Nanxuan Jiang[1], Zhou Zang[1], Xiaodan Guan[1], Xiaojun Ma[1], Zhuo Jia[2,3], Xiaorui Zhang[1], Yanting Zhang[1], Kangning Huang[4], Xiaocong Xu[5], Guolong Zhang[1], Jiming Li[1], Ran Yang[1], and Shujie Liao[1]

1 Key Laboratory for Semi-Arid Climate Change of the Ministry of Education, Lanzhou University, Lanzhou, 730000,China

2 College of Earth and Environmental Sciences, Lanzhou University, Lanzhou, 730000,China

3 Key Laboratory of Western China's Environmental Systems ( Ministry of Education), College of Earth and Environmental Sciences, Lanzhou University, Lanzhou, 730000, China

4 Yale School of Forestry and Environmental Studies, Yale University, New Haven, CT 06511

5 School of Geography and Planning, and Guangdong Key Laboratory for Urbanization and Geo-simulation, Sun Yat-sen University, Guangzhou, 510275, China

*Corresponding author: Jianping Huang; phone: 0931-8914139;
Email: hjp@lzu.edu.cn

Atmos. Chem. Phys. Discuss., https://doi.org/10.5194/acp-2017-890
Manuscript under review for journal Atmos. Chem. Phys.
Discussion started: 1 December 2017


Atmospheric Chemistry and Physics Discussions
Open Access
EGU

## Abstract

Dust emissions refer to the spatial displacement of dust particles from wind forcing, which is a key component of dust circulation. It plays an important role in the energy, hydrological, and carbon cycles of the Earth's systems. However, most dust emission schemes only consider natural dust, neglecting anthropogenic dust induced by human activities, which led to large uncertainties in quantitative estimations of dust emissions in numerical modeling. To fully consider the mechanisms of anthropogenic dust emissions, both "indirect" and "direct" anthropogenic dust emission schemes were constructed and developed in the study. Cloud-Aerosol Lidar and Infrared Pathfinder Satellite Observations (CALIPSO) retrievals were used to constrain the simulations at global scale. The results showed that the schemes reasonably reproduced the spatio-temporal distributions of anthropogenic dust from 2007 to 2010. The high centers of anthropogenic dust emission flux appeared in India, eastern China, North America, and Africa range from 0.9 to 11 μg $m^{-2}$ $s^{-1}$. Compared with natural dust emissions, indirect anthropogenic dust emissions have indistinctive seasonal variation, with differences less than 3.2 μg $m^{-2}$ $s^{-1}$. Pasturelands contribute higher anthropogenic dust emissions than croplands, with emissions of approximately 6.8 μg $m^{-2}$ $s^{-1}$, accounting for 60% of indirect anthropogenic dust emissions. Moreover, average anthropogenic dust emissions in urban areas have a value of 13.5 μg $m^{-2}$ $s^{-1}$, which is higher than those in rural areas (7.9 μg $m^{-2}$ $s^{-1}$). This study demonstrates that the environmental problems caused by anthropogenic dust in urban areas cannot be ignored.

**Key words:** Anthropogenic dust, Indirect anthropogenic dust emission, Direct anthropogenic dust emission, Dynamic land cover, Cropland, and Pastureland

Atmos. Chem. Phys. Discuss., https://doi.org/10.5194/acp-2017-890
Manuscript under review for journal Atmos. Chem. Phys.
Discussion started: 1 December 2017


## 1. Introduction

Dust emissions are the result of a key process in the dust cycle that determines long-term transport, dry/wet deposition, radiation forcing, and other dust-related processes at both regional and global scales (Tegen and Fung, 1994; Gong et al., 2003, 2004; Han et al., 2004, 2010, 2012, and 2013; Shao et al., 2004, 2011; Huang et al., 2006a, b, c; Chen et al., 2013, 2014a, b; Li et al., 2016). Scientists have been constructing and developing dust emission schemes for simulation studies since the 1980s. Based on different assumptions and simplifications, Zender et al. (2003), Han et al. (2004), and Shao et al. (2006, 2011) divided dust schemes into three categories: empirical schemes, schemes based on simplified physical processes, and schemes based on detailed micro-physical processes. The development of dust schemes has deepened our understanding of dust-related processes and dust's influences on the environment and the climate at the regional and global scales (Gong et al., 2006; Zhao et al., 2010, 2013; Huang et al., 2007, 2014; Chen et al., 2014, 2017a, b; Liu et al., 2016).

Current studies on simulated dust emissions have mostly focused on natural dust. There remains a gap with regard to simulating dust emissions induced by human disturbances. In the early 1990s, Penner et al. (1994) and Tegen and Fung (1995) suggested that it was inaccurate to classify dust aerosols as natural aerosols. Dust aerosols should be classified as either natural dust or anthropogenic dust according to its source region. Natural dust emissions essentially originate from natural dust source regions. Sufficiently strong winds occur over bare soil surfaces and dust particles are lifted and emitted into the atmosphere (Shao et al., 2004; Ginoux et al., 2012). Anthropogenic dust can be interpreted as dust emitted through modifying or disturbing soil particles through direct and indirect human activity (Penner et al., 1994; Tegen and Fung, 1995; Huang et al., 2015). Furthermore, anthropogenic dust emissions are mainly derived from wind erosion in anthropogenic dust land use due to the dryland vulnerability (i.e., "indirect anthropogenic dust emissions") (Xi et al., 2015) and human endeavors directly including urban activities, industrial activities (e.g., construction, cement production, and transportation), and farming (e.g., harvesting, plowing, and overgrazing) (i.e., "direct anthropogenic dust emissions") (Moulin and Chiapello, 2006; Munkhtsetseg et al., 2017).

The contributions of anthropogenic dust to the total dust mass cannot be ignored (Ginoux et al., 2012; Huang et al., 2006a, b, 2015, 2016; Xi et al., 2016; Guan et al., 2015, Chen et al., 2014b, 2017c; Kang et al., 2015; Luan et al., 2017). Compared with naturally occurring dust, anthropogenic dust particles can more easily be emitted continuously from anthropogenic dust source regions, mostly because these areas contain freshly exposed soil with more fine materials (Tegen and Fung, 1995; Zheng et al., 2016) which makes the soil more susceptible to erosion due to the lower threshold friction velocity (Tegen et al., 2004). Such large amounts of anthropogenic dust particles are likely to have a considerable impact on regional climate variations. Previous studies have pointed out that the radiative forcing induced by anthropogenic dust is likely to be equivalent to other anthropogenic aerosols, although these simulations had a large degree of uncertainty (Sokolik and Toon, 1996). Other studies have found that anthropogenic dust can have an impact on nutrient deposition (Mahowald et al., 2008) and regional snowpack (Ye et al., 2012; Semborski, 2013; Zhao et al., 2013). Therefore, quantitative estimation of anthropogenic dust emission is crucial to reinforce the understanding of the dust cycle and its climate effects at the regional and global scale, and decrease the uncertainties of dust emission flux in the numerical modellings.

At present, the uncertainty of determining anthropogenic dust sources and constructing dust emission schemes has led to larger biases in the estimation of anthropogenic dust emissions. This research has noted that simulated anthropogenic dust contributions to the total dust loading mass have ranged from 10% to 60% (see Table 1). Below, we have summarized several key reasons for such large uncertainties.

**First, lacking of observation constraints on estimations of anthropogenic dust.** Due to the difficulties in detecting and discriminating of anthropogenic dust, simulated anthropogenic dust has always been limited by a lack of observational constraints. Ground observations can not capture the anthropogenic dust emission well because observed dust loading is a mixture of natural dust and anthropogenic dust. With the development of remote sensing and inversion algorithms, Ginoux et al. (2010) identified anthropogenic and natural dust sources in western Africa based on Moderate Resolution Imaging Spectroradiometer (MODIS) Deep Blue aerosol products in combination with land use data. This approach indicated that anthropogenic dust accounts for 25% of all mineral aerosols (Ginoux et al., 2012). However, their retrieval method was only applicable over bright surfaces in the visible wavelength and was unable to properly exclude natural dust aerosols due to the lack of vertical information. Huang et al. (2015) proposed a new technique to identify anthropogenic dust using Cloud-Aerosol Lidar and Infrared Pathfinder Satellite Observations (CALIPSO). Their estimated anthropogenic dust contribution was approximately 25% of global dust loading and 52% of it in semi-humid and semi-arid areas. These studies provide valuable observations that could be used to constrain simulated anthropogenic dust in numerical modeling.

**Second, neglecting the influence of dynamic land surface in the anthropogenic dust emission.** Most dust emission schemes have employed "climatological" land cover to identify dust source distributions but have neglected temporal variations linked to surface bareness (Kim et al., 2013, 2017). Compared with natural dust sources, anthropogenic dust sources have diverse feature types, scattered distribution, and high spatiotemporal variability. Therefore, anthropogenic dust source regions have more significant seasonal and inter-annual variations (Huang et al., 2015). These dynamic land cover changes should be considered when estimating anthropogenic dust sources. There is a statistical relationship between the normalized difference vegetation index (NDVI) and dust concentrations in dust source regions (Zender and Kwon, 2005). Thus, Kim et al. (2013) developed a time dependency feature for their dust source function in the Goddard Chemistry Aerosol Radiation and Transport (GOCART) model simulations using NDVI from the advanced very high-resolution radiometer (AVHRR) from 2002 to 2007. Xi et al. (2016) further used the dynamic dust source functions from Kim et al. (2013) to quantify anthropogenic dust emissions from agricultural land use.

**Third, neglecting the direct anthropogenic dust emissions induced by human activities.** Previous studies have commonly employed indirect anthropogenic dust emissions in agricultural land use (e.g., Xi et al., 2016). However, rapid urbanization and increasingly frequent human activity are likely to produce large amounts of anthropogenic dust particles in urban areas. Observations have shown that anthropogenic dust mass loading is stronger than natural dust loading in densely populated regions with a high level of human activity. For example, anthropogenic dusts accounts for more than 91.8% and 76.1% of the total dust loading in east China and India, respectively (Huang et.al., 2015). Guan et al. (2016) further pointed out that direct anthropogenic dust loading in congested areas where the population density is more than 90 people per square kilometer (people km$^{-2}$) is much larger than the indirect anthropogenic dust from croplands, pasturelands, and grasslands. Taking East Asia as an example, the population density has been growing significantly over the past half century. The urban population in East Asia is approximately 60.1% of the entire population of East Asia, which was more than half the global urban population until 2015 (Mitchell et al., 2016). Thus, direct anthropogenic dust emission scheme should be considered in dust modeling.

In this study, we estimated the spatial distribution of anthropogenic dust emissions at global scale from 2007 to 2010. This paper is organized as follows.

Methods and datasets are described in Section 2. Model evaluation and discussion of anthropogenic dust emissions from 2007 to 2010 are presented in Sections 3. A broader discussion and conclusions are presented in Section 4.

## 2. Methods and datasets

### *2.1 Methods*

Previous research has found that human endeavors can directly and indirectly contribute to anthropogenic dust uplift (Zender et al., 2004; Xi et al., 2016). According to differences in the mechanisms of anthropogenic dust emissions, we divided these dust emissions into direct and indirect anthropogenic dust uplift, respectively. We used different methods to simulate these two anthropogenic dust emission sources using observations and reanalysis data, respectively.

***(1) Indirect anthropogenic dust emission***

To isolate the role of meteorology from the land surface effects, Marsham et al. (2011) simplified the dust emission scheme developed by Marticorena and Bergametti (1995). The scheme neglected differences from using wind speed at 10 m rather than at threshold velocity (Marsham et al., 2011). Instead, they substituted the threshold wind velocity by a constant of 7 m $s^{-1}$. Although this approach neglected the second-order effects of stability and roughness, it is a simple and easy method to better quantify the effects of meteorology on dust emissions at global scale over long time periods (Cakmur et al., 2004). Cakmur et al. (2004), Marsham et al. (2011), and Evan et al. (2016) pointed out that this dust emission scheme could reflect potential dust emissions, which is closely related to real-world dust emissions.

Indirect anthropogenic dust emissions are commonly caused by the erosive force of wind over anthropogenic land surfaces. Therefore, we used the simplified dust emission scheme by Marticorena and Bergametti (1995) to estimate the indirect anthropogenic dust emission. The influence of dynamic land surface in the indirect anthropogenic dust emission was also considered.

Indirect anthropogenic dust emission flux $G_I$ (μg m$^{-2}$ s$^{-1}$) was calculated as follows:

$$G_1 = C \times S_{ad} \times u^3 \times (1 + \frac{u_t}{u}) \times (1 - \frac{u_t^2}{u^2}), \text{ if } u > u_t, \quad \mathbf{(1)}$$

where $C$ is an empirical proportionality constant (units: μg s$^2$ m$^{-5}$), $S_{ad}$ is the anthropogenic dust source function, $u$ is the wind speed at 10 m, and $u_t$ is the threshold velocity depending on surface characteristics (when $u > u_t$, soil particles are possibly being uplifting). Here, we chose $u_t$ = 6.5 m s$^{-1}$ according to Tegen et al. (2004) because human disturbances make the soil more susceptible to erosion.

The anthropogenic dust source function $S_{ad}$ represents the probability of indirect anthropogenic dust uplifting with a range between 0 and 100. $S_{ad}$ is calculated by multiplying the accumulated sediments $H$, with the surface bareness percent $B$ (Kim et al., 2013). Notable, $S_{ad}$ is only calculated for anthropogenic land covers (i.e., $C_4$ croplands and $C_4$ pasturelands; for detailed information please see Section 2.2.2). Furthermore, high values of snow cover and soil moisture are excluded in this $S_{ad}$ calculation. Surface bareness $B$ is a "static" function that did not reflect the seasonal and inter-annual variations of land cover and soil bareness in the most research of dust emission schemes (e.g., Ginoux et al., 2001; Chin et al., 2002). Chen et al., (2014b, 2017a) pointed out that the "static" dust source function could lead to uncertainty in the simulated seasonal dust emission flux. Kim et al. (2013, 2017) used the NDVI to obtain a dynamic dust source function in Sahel, choosing 0.15 as the threshold to discriminate the bare ground. Hence, the NDVI of 0.15 was chosen to define the threshold surface bareness in this study. Next, $B$ was calculated as the ratio of the number of NDVI pixels below 0.1 (i.e., $N_{<0.15}$) to the total number of NDVI pixels within the 1° × 1° grid cell (i.e., $N_{total}$) as follows:

$$B = \frac{N_{<0.15}}{N_{total}} \quad \mathbf{(2)}$$

Additionally, topographical depression features *H*, is defined as the probability of having accumulated sediments in grid cell *i* of altitude $z_i$ (the local averaged surface elevation). A map of *H* was constructed from the altitude in the grid cell *i* relative to the altitude of the surrounding areas within a 5° × 5° grid in this study (Ginoux et al., 2001; Kim et al., 2013).

$$H = \left(\frac{Z_{max} - Z_i}{Z_{max} - Z_{min}}\right)^5 \qquad \textbf{(3)}$$

where $z_{max}$ and $z_{min}$ are the maximum and minimum elevations within the 5° ×5°grid, respectively, and $z_i$ is the altitude in the grid cell *i*.

***(2) Direct anthropogenic dust emissions***

Direct anthropogenic dust emissions primarily originate from human activities and urbanization processes, such as city construction, cement production, traffic, and transportation. Population density, urbanization, and the levels of regional economic development, as important driving factors, should be contained in the calculating direct anthropogenic dust. The STIRPAT (the stochastic impacts by regression on population (P), affluence (A), and technology (T)) model is widely used to analyze the effects of driving forces on a variety of environmental impacts (Dietz and Rosa, 1997; Soulé and DeHart, 1998; Shi, 2003; and York et al., 2003). Here, we employed the STIRPAT model to calculate direct anthropogenic dust emissions based on the population density, compounded nighttime light index (CNLI), and Engel coefficient. The direct anthropogenic dust emissions, $G_2$ (μg m$^{-2}$ s$^{-1}$), was calculated using the following equation:

$$G_2 = a \times P^b \times CNLI^c \times EC^d \qquad (4)$$

where a is an empirical proportionality constant (units: μg s$^2$ m$^{-5}$); and b, c, and d represent the driving force indices. *P* represents the population density, *CNLI* (see Section 2.2.4) represents the urbanization level, and *EC* is the Engel coefficient, indicating the proportion of total food expenditure to total amount of consumer spending, which represents economic development. Converting Eq. (5) into a linear form, we have

$$\ln(G_x) = \ln a + b\ln(P) + c\ln(CNLI) + d\ln(EC) \qquad (5)$$

To determine the coefficients for a, b, c, and d, we used the least squares method based on the anthropogenic dust column from CALIPSO, together with the independent variables of P, CNLI, and EC to determine that b=0.1, c=0.1, and d=1.6. In the regression calculation using the least squares method, we validated the well-parameterization for equation with a reasonable error (root mean square error=1.21) and a good fit (coefficient of determination=0.26). At a significance level of $\alpha$ =0.005, all of the independent variables passed an F-test, indicating that direct anthropogenic dust emissions showed good agreement with the population density, CNLI, and EC. Notably, high vales of soil moisture were excluded, because they reinforced inter-particle cohesion forces thus limiting the probability of dust emissions (Fécan et al., 1998).

## 2.2 Datasets

### *2.2.1 ERA-Interim*

We used the reanalysis product ERA-Interim from the European Centre for Medium-Range Weather Forecasts (ECMWF) in this study. The ERA-Interim project was conducted to replace ERA-40 with a new atmospheric reanalysis procedure, which improves the quality of the reanalysis products in various ways, such as data selection, quality control, bias correction, and performance monitoring (Dee et al., 2011). ERA-Interim covers the period from 1 January 1979 onwards, and continues to be extended forward in near-real time, with a time step of 6 h. Furthermore, it is available for global statistics covering both ocean and land at a spatial resolution of 0.5°×0.5°.

According to Largeron et al. (2015), compared with two other global reanalysis datasets, NCEP-CFSR and MERRA, ERA-Interim effectively capture the spatial and temporal variations of wind speed at 10 m, which makes it the optimal reanalysis product to calculate potential dust uplifting. The annual

Atmos. Chem. Phys. Discuss., https://doi.org/10.5194/acp-2017-890
Manuscript under review for journal Atmos. Chem. Phys.
Discussion started: 1 December 2017


Atmospheric Chemistry and Physics Discussions

bias of ERA-Interim is 0.27 m $s^{-1}$. MERRA and NCEP-CFSR have values of 0.70 m $s^{-1}$ and −0.62 m $s^{-1}$, respectively, compared with observations from the network of African Monsoon Multidisciplinary Analyses (AMMA) (Redelsperger et al., 2006). Therefore, wind speed at 10 m from the ERA-Interim datasets was chosen to calculate indirect anthropogenic dust emission flux in this study.

### *2.2.2 Land cover datasets*

Land cover datasets from Meiyappan and Jain (2012) incorporate 28 types of land cover, including 16 types of natural land cover (e.g., forests, grasslands, shrubs, etc.) and 12 types of land cover disturbed by human activities (e.g., secondary forests, croplands, pasturelands, and urban environments) (Table 2). This land cover dataset, combined with the Historical Database of the Global Environment (HYDE 3.1) (Klein et al., 2010, 2011), wood harvest data, and urban land data, was used to construct the anthropogenic land cover map including cropland, pastureland, and urban regions, which provide dynamic land cover variations at 0.5°×0.5° resolution from 1770 to 2010. Friedl et al. (2010) pointed out that the datasets effectively captured the spatial and temporal distributions of land cover at global scale compared with MODIS retrievals from 2000 to 2005.

Huang et al. (2015) decided to limit the mapping to three surface types (croplands, grasslands, and cropland mosaics) to define anthropogenic dust source regions based on the land cover products from MODIS Collection 5.1. Here, we chose both cropland and pastureland as indirect anthropogenic dust source types. In addition, according to differences in photosynthesis dark reactions, vegetation was divided into $C_3$ and $C_4$ vegetation (O'Leary 1981). $C_3$ vegetation refers to vegetation whose initial product of the photosynthesis carbon cycle is 3-phosphoglycerate including almost all trees, most types of shrubs, and cold-season turf grass. $C_4$ vegetation refers to vegetation whose initial product of the photosynthesis carbon cycle is not 3-phosphoglycerate but four-membered carbons, like malic acid or aspartic acid. $C_4$ vegetation mainly consists of warm-season turf grass (Sage and Monson, 1999). Research has noted that $C_4$ vegetation is largely distributed in regions that are primarily deserts, such as the Gobi Desert, or grasslands with sparse vegetation. $C_4$ vegetation has a weak ability to fix dust particles, thus it benefits from dust emissions. Schefuß et al. (2003) found the $C_4$ vegetation could produce more frequent dust emissions in the Sahara and Sahel deserts compared with $C_3$ vegetation. Huang et al. (2000) also revealed that there was a dominant contribution of surfaces covered by $C_4$ vegetation to dust emissions compared with surfaces covered with other vegetation. Therefore, to better quantify indirect dust emission flux, we further chose regions that were primarily $C_4$ croplands and $C_4$ pasturelands as indirect anthropogenic dust source regions according to the land cover data provided by Meiyappan and Jain (2012).

### *2.2.3 Population data*

Population data was obtained from the Gridded Population of the World dataset, version 3 (GPWv3, http://sedac.ciesin.columbia.edu/gpw), which is supported by the Center for the International Earth Science Information Network and the Centro Internacional de Agricultural Tropical. GPWv3 provides spatial distributions of population density at global scale. The spatial resolution is 0.5°×0.5° and the time resolution is every 5 years from 1990 to 2010 (i.e., the population data are for the years 1990, 1995, 2000, 2005, and 2010).

### *2.2.4 Compounded night light index (CNLI)*

Researchers have always utilized nighttime light, based on the Defense Meteorological Satellite Program/The Operational Linescan System (DMSP/OLS), to extract spatial distribution characteristics of urban areas (Elvidge et al., 1997). The DMSP satellite carries the OLS, which has a visible channel and an infrared channel with gray levels ranging from 0 to 63 and 0 to 255, respectively. The OLS has a strong photoelectric amplification capacity and can obtain fire data and upper atmospheric source data, such as the appearance of the northern lights. Nighttime light products are derived from the average visible band digital number (DN) of cloud-free light detections multiplied by the percent frequency of light detection. Therefore, city lights can be recorded in the nighttime imagery. This has been widely used abroad to detect urban areas, supervise fires, etc. (Sutton, 1997; Elvidege et al., 1997, 2013; Lo et al., 2001).

To simulate direct anthropogenic dust emissions caused by human activities, we estimated the CNLI from 2007 to 2010 based on nighttime light datasets that recognize urbanization levels at global scale. The CNLI proposed by Zhuo et al. (2003) represents urbanization level with a value between 0 and 1. CNLI is defined as the ratio of lit urban areas to the whole region R and average night light brightness I within a 1° × 1° grid cell as follows:

$$\mathrm{CNLI} = \mathrm{I} \times \mathrm{R} \qquad \textbf{(7)}$$

R is computed using the following formula (8):

$$R = \frac{Area_N}{Area_{total}} \qquad \textbf{(8)}$$

where $Area_N$ is the area of lit urban areas in a region and $Area_{total}$ is the 1° × 1° grid in the calculation. Night light brightness $I$ is presented below:

$$I = \frac{1}{N_L \times DN_M} \times \sum_{i=P}^{DN_M} (DN_i \times n_i) \qquad \textbf{(9)}$$

where the digital number ($DN_i$) is the $i$th gray level of the $DN$ value within the 1°×1° grid; $n_i$ is the total number of lit pixels belonging to the $i$th gray level; and $P$ is the threshold value representing the beginning of an increasing urbanization trend. $DN_M$ is the maximum potential $DN$ value within the 1° × 1° grid, and $N_L$ is the number of lit pixels whose $DN$ value is between $P$ and $DN_M$ (i.e., the number of lit pixels).

### *2.2.5 CALIPSO*

CALIPSO launched on 28 April 2006 and combines an active Lidar instrument with passive infrared and visible images to delineate the vertical profiles and properties of aerosols and clouds at a global scale. This tool provides new insights into the influence of clouds and aerosols on Earth's weather, climate, and air quality (Winker et al., 2007; Hu et al., 2007a, 2007b, 2009). This study used CALIPSO retrievals to calculate the anthropogenic dust optical depth (ADOD) and the anthropogenic dust loading, following the approach of Huang et al. (2015). The first step was to detect the total dust column from CALIPSO retrievals, and the second step was to select the potential dust source regions based on the datasets from Meiyappan and Jain (2012). Then we calculated the height of the planetary boundary layer (PBL) because most anthropogenic dust particles accumulate under the PBL (Jordan et al., 2010; Yu et al., 2012). Finally, we calculated the anthropogenic dust optical depth and the anthropogenic dust column. A detailed description of this anthropogenic dust detecting procedure based on CALIPSO retrievals can be found in Huang et al. (2015).

## *3. Results*

### *3.1 Indirect anthropogenic dust emission*

The land cover datasets used in this study reproduced the spatial distributions of anthropogenic land cover over the past 100 years. The dominant 17 types of land cover from Meiyappan and Jain (2012) are shown in Figure 1a. Land cover types can be divided into anthropogenic land use and natural land use (Table 1). Croplands were mainly distributed in the eastern and central North America, east and central Asia, as well as throughout Europe. Pasturelands dominate central North America, eastern South America, central Asia, and the southern Sahara.

In this study, we only included $C_4$ croplands and $C_4$ pasturelands as potential indirect anthropogenic dust sources (Figure 1b and 1c), demonstrating the wide spread of indirect anthropogenic dust. $C_4$ croplands have common crops, such as corn and sorghum (Ehleringer and Cerling, 2002), that are distributed extensively throughout the tropics and subtropics in regions such as central and eastern North America, the southern Sahara, southern Europe, eastern China, and western India. $C_4$ pasturelands are also mainly distributed in the tropics and subtropics, in regions such as central North America, the southern Sahara Desert, the northern region of South America, and the southern region of the Yangtze River Basin in China. Its turf grass is mainly comprised of poapratensis and fescue grasses (Ehleringer and Cerling, 2002). Although $C_4$ pasturelands are comparatively less extensive than $C_4$ croplands in Europe and the central and east of Asia, the proportion of $C_4$ pasturelands is significantly higher in the east of South America, the southern region of the Sahara Desert and Africa, as well as western India. For example, the percentage of $C_4$ pasturelands can reaches up to 50% in South Africa and South America, while $C_4$ croplands rarely occupy more than 20% of the total area.

The NDVI values indicate that there are significant seasonal variations in vegetation cover and surface bareness, especially in anthropogenic land areas (Figure 2). On the whole, NDVI in July is generally higher than that in January in the Northern Hemisphere, where the difference can reach up to 0.3. The variations in NDVI are comparatively slight in deserts like the Sahara, western regions of Asia, and the Taklimakan Desert in Australia, all with differences of approximately 0.1. Because the two hemispheres have opposite seasons and that special climate characteristics were measured at regional scale, NDVI values decreased from January to July in a few regions like southern Africa (Figures 2a and b). This is consistent with previous results from Kim et al. (2013).

The global surface bareness map was constructed using NDVI data (Figures 2c and d). The surface bareness in cold seasons is more extensive and intensive than in warm seasons, especially in the south Sahara Desert and in central and east Asia. Interesting, the bareness in Australia is the opposite due to the unique climate and vegetation characteristics at the regional scale. This is likely because evergreen trees dominate the northern part of Australia and tend to be denser in July. Moreover, some of the regions, like southwest Australia, experience a Mediterranean climate in which vegetation grows thicker in July (Scott et al., 1993; Bowman et al., 2005).

The indirect anthropogenic dust source function $S_{ad}$ reflects the probability of indirect anthropogenic dust uplifting, which is constructed using soil bareness (Figures 2c and d) and topographic features (Figure 3b) in $C_4$ croplands and $C_4$ pasturelands. The higher topographic depression $H$ reflects flatter regions, which is more likely to have accumulated sediment (Figure 3b). In Figures 3c and 3d, we can see that $S_{ad}$ experienced significant variation, and was distributed in central and east Asia, the southern Sahara, and western North America. It was more widespread in January than in July in the Northern Hemisphere, especially in western regions of North America, the southern Sahara, eastern China, and central Asia. The Southern Hemisphere tends to experience the opposite of these variations, although Australia is an exception, as discussed earlier.

The global distribution of seasonal indirect anthropogenic dust emission flux from 2007 to 2010 is shown in Figure 4. The highest centers of indirect anthropogenic dust emission flux occurred in North America (1.80 μg $m^{-2}$ $s^{-1}$), India (3.39 μg $m^{-2}$ $s^{-1}$), and eastern China (2.60 μg $m^{-2}$ $s^{-1}$) due to the wide range of $C_4$ croplands and $C_4$ pasturelands (Figure 1). As human disturbances can make soils more susceptible to erosion, anthropogenic land cover types contributed a considerable proportion of indirect anthropogenic dust to total anthropogenic dust (Justice et al., 1996; Huang et al., 2015). Indeed, indirect anthropogenic dust emission flux consistently showed indistinctive seasonal variation compared with natural dust emission flux. The variations in anthropogenic dust emission flux over four seasons were no more than 0.64 μg $m^{-2}$ $s^{-1}$.

**3.2 *Direct anthropogenic dust emission***

Atmos. Chem. Phys. Discuss., https://doi.org/10.5194/acp-2017-890
Manuscript under review for journal Atmos. Chem. Phys.
Discussion started: 1 December 2017




Huang et al. (2015) and Guan et al. (2016) suggested that anthropogenic dust has a close relationship with population density and the level of urbanization. Therefore, to calculate direct anthropogenic dust emissions, we used population density values, the CNLI, and the Engel Coefficient (EC), which are shown in Figure 5. The values for human population density are as high as 400 people km$^{-2}$ in eastern China. Mumbai, located in northern India, has the largest population density, which were 29,650 people km$^{-2}$ in 2010. CNLI is the light index reflecting the development of urbanization (Figure 5b). The high centers of CNLI appeared in India, the east of China, Europe, and the east of North America, indicating a higher urbanization level in these regions, which showed good agreement with the population density.

Moreover, direct anthropogenic dust emissions also depend on economic development. Huang et al. (2015) found that direct anthropogenic dust was negatively correlated with regional economic progress. Hence, EC indicates the proportion of the total food expenditure to the total amount of consumer spending, as this plays an essential role in evaluating the living standard of residents and the region's stage of economic development (Zhang et al., 2010). Previous studies have showed that a region with an EC value higher than 0.6 can be defined as poverty stricken. When the value falls between 0.5 and 0.6, the population is barely meeting its daily needs. If the value falls between 0.4 and 0.5, there is a moderately well-off standard of living. If the value falls between 0.3 and 0.4, there is well-to-do standard of living. Finally, if the value falls below 0.3, the population is generally quite wealthy (Zhang et al., 2010). As shown in Figure 5a, the economic development of a country is negatively correlated with EC. The United States, England, and France are the most advanced developed countries in the world with EC values as low as 0.08, 0.13, and 0.17, respectively. China and India are both developing countries with an EC value of 0.22 and 0.26, respectively.

Direct human activities dominate anthropogenic dust emissions. Magnitudes of direct anthropogenic dust emission flux are nearly three to four times higher than that of indirect anthropogenic dust emission flux (Figure 6). Direct anthropogenic dust emission flux shows clear regional heterogeneity. Developing countries, such as India and China, contribute the greatest amount of direct anthropogenic dust (up to 4.3 μg $m^{-2}$ $s^{-1}$ and 3.0 μg $m^{-2}$ $s^{-1}$, respectively) due to their incomplete industrial structures, city construction, and less restrictive environmental regulations. Outside of these two countries, in densely populated regions of developed countries, the average direct anthropogenic dust emission flux is comparatively less at approximately 1.6 μg $m^{-2}$ $s^{-1}$ because city development and environmental policies are more mature.

### 3.3 *Total anthropogenic dust emission*

Total anthropogenic dust emissions are overlaid by both direct and indirect anthropogenic dust. Figure 7 shows the simulated seasonal variations of anthropogenic dust emission flux at the global scale. The global annual mean anthropogenic dust column was approximately 0.11 g $m^{-2}$, and in regions like India, it could reach up to 0.87 g $m^{-2}$. It is evident that the simulated spatial distribution of anthropogenic dust emissions is highly consistent with that produced by CALIPSO retrievals (Figure 8). Anthropogenic dust emission flux has indistinctive seasonal variation compared with natural dust emissions due to the main contributions of human activities in urban regions (Huang et al., 2015). The high centers of anthropogenic dust emission flux appear in eastern China, India, North Africa and North America, which is highly consistent with that of the anthropogenic dust column calculated by Huang et al. (2015) and Guan et al. (2016). However, the simulations underestimated the anthropogenic dust emissions in North America compared with CALIPSO retrievals due to the bias of estimating urbanization. Furthermore, Figure 9 shows the normalization anthropogenic dust from CALIPSO retrievals and our simulations in China, India, and North and South America. The simulations capture the differences of these three high anthropogenic dust regions. The magnitude of anthropogenic dust in India is highest due to the main contributions of direct anthropogenic dust emissions; it is second highest in China and lowest in the United States.

Compared with natural dust source regions, anthropogenic dust source regions are more complicated due to diverse types, scattered distribution, and high spatio-temporal variations. Divergences in anthropogenic land cover types are induced by the concept of "people managed" areas (Meiyappan et al., 2014). Cropland, pastureland and urban belong to human managed land area. Quantitative estimates of anthropogenic dust emissions in different land cover types are crucial to reinforce the understanding of dust emissions in anthropogenic land cover. For three major anthropogenic land covers, the contribution of anthropogenic dust emissions from croplands, pasturelands, and urban areas to the total anthropogenic dust column is 20.76%, 28.38%, and 50.86%, respectively (Figure 10), indicating that direct anthropogenic dust emissions from urban areas play a dominant role in anthropogenic dust. Pasturelands includes pastures and artificially sparse grasslands, which contribute higher anthropogenic dust emissions than croplands due to the more intense distributions and higher anthropogenic dust source functions in $C_4$ pastureland compared with those of $C_4$ croplands (Figure 1, Figure 3).

Further, although rural areas is larger than urban, anthropogenic dust emissions (13.54 μg $m^{-2}$ $s^{-1}$) in urban areas is higher than that in rural areas (7.89 μg $m^{-2}$ $s^{-1}$), suggesting that anthropogenic dust is more likely produced in urban areas than that in remote and rural areas (Figure 11). Therefore, policymakers should be paying much more attention to the control of air pollutions in urban areas. Further, anthropogenic dust emissions (13.54 μg $m^{-2}$ $s^{-1}$) in urban areas is higher than that in rural areas (7.89 μg $m^{-2}$ $s^{-1}$), suggesting that anthropogenic dust is more likely produced in urban areas than that in remote and rural areas (Figure 11). It is because that the larger bareness, more intensive population and high value of EC as well as CNLI in urban areas which result in both greater direct anthropogenic dust emission and indirect anthropogenic dust emission in urban than these in rural areas. Recently year, with increasing numbers of people who have migrated from rural areas to urban areas, the imbalanced distribution of anthropogenic dust emissions will be intensified, causing more ecological pressure for urban areas. Moreover, there exist much more human activities in urban areas, such as urban construction, cement production, transportation, energy consumption, etc, which cause large direct anthropogenic dust emissions. Therefore, policymakers should be paying much more attention to the control of air pollutions in urban areas.

## *4. Discussions and conclusions*

The contribution of anthropogenic dust to the total atmospheric dust column is significant and should not be ignored (Huang et al., 2015). Previous dust emission modellings merely focused on the natural dust emissions and there is a great knowledge gap of the investigation of the anthropogenic dust emissions. There are more difficulties and uncertainties in anthropogenic dust emissions simulations compared with those in natural dust emissions, due to the diverse types, scattered distribution, and high spatio-temporal variability of anthropogenic dust sources (Xi et al., 2016). Thus, quantitative estimations of anthropogenic dust emissions are crucial to reinforce the understanding of the dust cycle and its climate effects, and decrease the uncertainties of dust emission fluxes in the numerical modellings. According to different anthropogenic dust emission mechanisms, both “indirect” and “direct” anthropogenic dust emission schemes were constructed and developed in the study, respectively.

Indirect anthropogenic dust emissions are caused by the erosive force of wind on anthropogenic land surfaces as croplands and pasturelands. The simplified dust emission scheme proposed by Marsham et al. (2011) was used to simulate seasonal variations of indirect anthropogenic dust emissions in this study. In addition, previous studies focused on dust emissions in identifying dust sources only retained the static land cover types (Ginoux et al., 2001; Kumar et al., 2014; Nabavi et al., 2017). However, the static land cover types cannot reflect the dynamic change of dust sources well owing to seasonal variations of sparse vegetation. Therefore, dynamic land cover changes were considered by the anthropogenic dust source function based on the NDVI datasets in the study. Generally, indirect anthropogenic dust emission fluxes consistently showed indistinctive seasonal variation compared with natural dust emission fluxes. The highest centers of indirect anthropogenic dust emission flux occurred in North America (1.80 μg $m^{-2}$ $s^{-1}$), India (3.39 μg $m^{-2}$ $s^{-1}$), and eastern China (2.60 μg $m^{-2}$ $s^{-1}$). Notably, pasturelands (including pastures and artificially sparse grasslands) contribute higher anthropogenic dust emissions than croplands, with emissions of approximately 6.8 μg $m^{-2}$ $s^{-1}$, accounting for 60% of indirect anthropogenic dust emissions.

Direct anthropogenic dust emissions primarily originate from direct human activities and urbanization processes. The mechanism of direct anthropogenic dust emission is quite different from that of indirect anthropogenic dust emissions. Population density and urbanization dominate the magnitude of direct anthropogenic dust emission fluxes (Guan et al., 2016). We utilized the STIRPAT model to simulate the spatial distribution of direct anthropogenic dust emissions from 2007 to 2010, taking the impacts of population, urbanization, and the economic development of a region into consideration. Results showed that direct anthropogenic dust emissions reflect regional heterogeneity. Developing countries such as India and China act as dominant direct anthropogenic dust source regions (up to 4.3 μg $m^{-2}$ $s^{-1}$ and 3.0 μg $m^{-2}$ $s^{-1}$, respectively) owing to their incomplete industrial structure, ongoing city construction, and less restrictive environmental regulations. For developed countries, lots of regions are a large urban agglomeration with dense population such as England in Europe and New York in North America, the magnitude of direct anthropogenic dust emission fluxes is comparatively less. The more mature city development and environmental policies are the less anthropogenic dust emit.

Total anthropogenic dust emissions consist of both direct and indirect anthropogenic dust emissions. Total anthropogenic dust has a wide spread and the high value centers are concentrated in areas with a large population density and intense human activities in developing countries, such as India and eastern China. It indicates that direct anthropogenic dust plays an important role in total anthropogenic dust that cannot be ignored. Especially, anthropogenic dust emissions in urban areas (13.5 μg $m^{-2}$ $s^{-1}$) are higher than those in rural areas (7.9 μg $m^{-2}$ $s^{-1}$), suggesting that there is a greater potential for higher anthropogenic dust emissions in urban areas than in rural or remote areas.

In addition, due to the difficulties in detecting and discriminating of anthropogenic dust, the previous studies about simulations of anthropogenic dust emission are poorly evaluated by observations. As a unique observational constrain of anthropogenic dust, Cloud-Aerosol Lidar and Infrared Pathfinder Satellite Observations (CALIPSO) retrievals were used to evaluate the simulations at global scale in the study. Huang et al., (2015) pointed out that anthropogenic dust is hard to lift up to the planet boundary layer for having a long-range transport, the anthropogenic dust column is generally contributed by the anthropogenic dust emissions in local regions. Therefore, we have compared the simulated anthropogenic dust emissions with the CALIPSO anthropogenic dust columns as noted in Huang et al. (2015) and Guan et al. (2016), without even having other observations. The comparisons indicated that the simulations captured the spatial distributions of CALIPSO anthropogenic dust well. In the future, the development of integrated systematic observations of anthropogenic dust in different land cover types is necessary for improving anthropogenic dust emission schemes and simulations.

Although anthropogenic dust emissions were simulated in the study under constrains of CALIPSO retrievals, some uncertainties are still exist. For one thing, various important factors are not considered in the direct anthropogenic dust scheme, such as the influence of city traffic, areas of urban roads, urban construction, urban development, and environmental policies. These factors will be considered in by developing more detailed direct anthropogenic dust emission schemes and constructing fugitive road dust emission inventories in our future study. For another, the indirect dust emission scheme only considered a few key factors that contribute to anthropogenic dust emissions in the paper. More complicated anthropogenic dust emission schemes, taking anthropogenic dust size distributions, soil moisture, chemical composition, etc into consideration, will be coupled with the Weather Research and Forecasting model with chemistry (WRF-Chem) model under constraints of satellite retrievals and ground observations.

***Acknowledgments***

We acknowledge Chun Zhao and Ben Yang for their help for this work. This research was supported by the Foundation for National Natural Science Foundation of China (No. 41775003; No. 41405003), Innovative Research Groups of the National Science Foundation of China (Grant No. 41521004) and )and the Foundation of Key Laboratory for Semi-Arid Climate Change of the Ministry of Education in Lanzhou University. We would like to thank Meiyappan, P. and Jain, A., for the land cover data used in this study. The Historical Land-Cover Change and Land-Use Conversions Global Dataset used in this study were acquired from NOAA"s National Climatic Data Center (http://www.ncdc.noaa.gov/).

## References:


Bowman, D. M. J. S., and Prior, L. D.: Why do evergreen trees dominate the Australian seasonal tropics? Australian Journal of Botany, 53 (5):379-399, doi: 10.1071/BT05022, 2005.

Cakmur, R.V., Miller, R.L. and Torres, O.: Incorporating the effect of small - scale circulations upon dust emission in an atmospheric general circulation model, J. Geophys. Res. Atmos., 109 (11) :2136-2142, doi: 10.1029/2003JD004067, 2004.

Chen, S. Y., Huang, J. P., Zhao, C., Qian, Y., Leung, R. L., and Yang, B.: Modeling the transport and radiative forcing of Taklimakan dust over Tibetan Plateau: A case study in the summer of 2006, J. Geophys. Res., 118, 797-812, doi: 10.1002/jgrd.50122, 2013.

Chen, S. Y., Zhao, C., Qian, Y., Leung, R. L., Huang, J. P., Huang, Z. W., Bi, J. R., Zhang, W., Shi, J. S., Yang, L., Li, D. S., and Li, J. X.: Regional modeling of dust mass balance and radiative forcing over East Asia using WRF-Chem, Aeolian Res., 15, 15-30, doi : 10.1016/j.aeolia.2014.02.001, 2014a.

Chen, S. Y., Huang, J. P., Qian, Y., Ge, J. M., and Su, J.: Effects of aerosols on autumn precipitation over Mid-eastern China, J. Trop. Meteor., 20, 242-250, doi: 10.3969/j.issn.1004-4965.2012.03.006, 2014b.

Chen, S. Y., Huang, J. P., Li, J. X., Jia, R., Jiang, N. X., Kang, L. T., Ma, X. J., and Xie, T. T.: Comparison of dust emission, transport, and deposition between the Taklimakan Desert and Gobi Desert from 2007 to 2011, Sci. China: Earth Sci., 60,1-18, doi: 1.01007/s11430-016-9051-0, 2017a.

Chen, S. Y., Huang, J. P., Qian, Y., Zhao, C., Kang, L. T., Yang, B., Wang, Y., Liu, Y. Z., Yuan, T. G., Wang, T. H., Ma, X. J., and Zhang, G. L.: An Overview of Mineral Dust Modeling over East Asia, J. Meteor. Res., 31, 633-653, doi: 10.1007/s13351-017-6142-2, 2017b.

Chen, S. Y., Huang, J. P., Kang, L. T., Wang, H., Ma, X. J., He, Y. L., Yuan, T. G., Yang, B., and Huang, Z. W., and Zhang, G. L.: Emission, transport and radiative effects of mineral dust from Taklimakan and Gobi Deserts: comparison of measurements and model results, Atmos. Chem. Phys., 17, 1-43, doi: 10.5194/acp-17-2401-2017, 2017c.

Chin, M., Ginoux, P., Kinne, S., Torres, O., Holben, B., Duncan, B.,Martin, R., Logan, J., Higurashi, A., And., and Nakajima, T.: Tropospheric aerosol optical thickness from the GOCART model and comparisons with satellite and Sun photometer measurements, J.

Atmos. Chem. Phys. Discuss., https://doi.org/10.5194/acp-2017-890
Manuscript under review for journal Atmos. Chem. Phys.
Discussion started: 1 December 2017


Atmospheric Chemistry and Physics Discussions

Atmos. Sci., 59(3), 461–483, doi: 10.1175/1520-0469(2002)059<0461:TAOTFT>2.0.CO;2, 2002.

Dietz, T., and Rosa, E.A.: Effects of population and affluence on CO2 emissions, Proceedings of the National Academy of Sciences of the United States of America, 94 (1) :175-9, doi: 10.1073/pnas.94.1.175, 1997.

Dee, D. P., Uppala, S., Simmons, M., A. J., Berrisford, P., Poli, P., Kobayashi, S., Andrae, U., Balmaseda, M. A., Balsamo, G., Bauer, P., Bechtold, P., Beljaars, A. C. M.,van de Berg, L.,Bidlot, J., Bormann, N., Delsol, C., Dragani, R., Fuentes, M., Geer, A. J., Haimberger, L., Healy, S. B., Hersbach, H., Hólm, E. V., Isaksen, L., Kållberg, P., Köhler, M., Matricardi, M., McNally, A. P., Monge-Sanz, B. M., Morcrette, J.-J., Park. B.-K., Peubey, C., Rosnay, P. de, Tavolato, C., Thépaut, J.-N., and Vitart, F.: The ERA-Interim reanalysis: configuration and performance of the data assimilation system, Quart. J. Roy. Meteor. Soc., 137 (656), 553-597, doi: 10.1002/qj.828, 2011.

Elvidge, C.D., Zhizhin, M., Hsu, F.C., Baugh, K.E.: VIIRS Nightfire: Satellite Pyrometry at Night, Remote Sensing., 5 (9) :4423-4449, doi: 10.3390/rs5094423, 2013.

Eheleringer, J. R., Cerling, T. E., C3 and C4 Photosynthesis, The Earth system: biological and ecological dimensions of global environmental change, vol 2, 186–190, 2002.

Fécan, F., Marticorena, B., and Bergametti, G.: Parameterization of the increase of the aeolian erosion threshold wind friction velocity due to soil moisture for arid and semi-arid areas, Annales Geophysicae., 17 (1) :149-157, doi: 10.1007/s00585-999-0149-7 Source: OAI, 1998.

Friedl, M. A., Sulla-Menashe, D., Tan, B., Schneider, A., Ramankutty, N., Sibley, A., and Huang, X.: MODIS Collection 5 global land cover: Algorithm refinements and characterization of new datasets, Remote Sens. Environ., 114(1), 168-182, doi: 10.1016/j.rse.2009.08.016, 2010.

Ginoux, P., Chin, M., Tegen, I., M.Prospero, J., Holben, B., Dubovik, O., and Lin S.-J.: Sources and distributions of dust aerosols simulated with the GOCART model, J. Geophys. Res., 106(D17), 20255–20273, doi: 10.1029/2000JD000053, 2001.

Ginoux, P., Garbuzov, D., and Hsu, N.C: Identification of anthropogenic and natural dust sources using Moderate Resolution Imaging Spectroradiometer (MODIS) Deep Blue level 2 data, J. Geophys. Res., 115 (D5) :458-473, doi: 10.1029/2009JD012398, 2010.

Ginoux, P., Prospero, J. M., Gill, T. E., Christina, N. H., and Zhao, M.: Global-scale attribution of anthropogenic and natural dust sources and their emission rates based on

MODIS Deep Blue aerosol products, Rev. Geophys., 50 (3), 3005, doi: 10.1029/2012RG000388, 2012.

Gong, S. L., Zhang, X. Y., and Zhao, T. L.: Characterization of soil dust aerosol in China and its transport and distribution during 2001 ACE-Asia: 2. Model simulation and validation, J. Geophys. Res., 108, 4262-4234, doi: 10.1029/2002JD002633, 2003.

Gong, S. L., Zhang, X. Y., Zhao, T. L., and Barrie, L. A.: Sensitivity of Asian dust storm to natural and anthropogenic factors, Geophys. Res. Lett., 31, L07210, doi: 10.1029/2004GL019502, 2004.

Gong, S. L., Zhang, X. Y., Zhao, T. L., Zhang, X. B., Barrie, L. A., McKendry, I. G., and Zhao, C. S.: A simulated climatology of Asian dust aerosol and its trans-Pacific transport. Part II: interannual variability and climate connections, J. Climate, 19, 104–122, doi: 10.1175/JCLI3606.1, 2006.

Guan, X., Huang, J., Guo, R., Yu, H., Lin, P., and Zhang, Y.: Role of radiatively forced temperature changes in enhanced semi-arid warming in the cold season over East Asia, Atmos. Chem. Phys., 15, 13777-13786, doi: 10.5194/acp-15-13777-2015, 2015.

Guan, X. D., Huang, J., Zhang, Y., Xie, Y., Liu, J.: The relationship between anthropogenic dust and population over global semi-arid regions, Atmos. Chem. Phys., 16, 5159–5169, doi: 10.5194/acp-16-5159-2016, 2016.

Han, Z. W., Ueda, H., Matsuda, K., Zhang, R. J., Arao, K., Kanai, Y., Hasome, H.: Model study on particle size segregation and deposition during Asian dust events in March 2002, J. Geophys. Res., 109, 4321-4339, doi: 10.1029/2004JD004920, 2004.

Han, Z. W.: Direct radiative effect of aerosols over East Asia with a regional coupled climate/chemistry model, Meteor.Z., 19, 287–298, doi: 10.1127/0941-2948/2010/0461, 2010.

Han, Z. W., Li, J. W., Xia, X. G, Zhang, R. J.: Investigation of direct radiative effects of aerosols in dust storm season over East Asia with an online coupled regional climate-chemistry-aerosol model, Atmos. Environ., 54 (4), 688–699, doi: 10.1016/j.atmosenv.2012.01.041, 2012.

Han, Z. W., Li, J. W., Guo, W. D., Xiong, Z., Zhang, W.: A study of dust radiative feedback on dust cycle and meteorology over East Asia by a coupled regional climate-chemistry-aerosol model, Atmos. Environ., 68 (1), 54-63, doi: 10.1016/j.atmosenv.2012.11.032, 2013.

Hu, Y. X., Vaughan M., Liu, Z. Y., Lin, B., Yang, P., Flittner, D., Hunt, B., Kuehn, R., Huang, J. P., Wu, D., Rodier, S., Powell, K., Trepte, C., and Winker, D.: The depolarization-attenuated back scatter relation: CALIPSO lidar measurements vs. theory, Opt. Express, 15, 5327–5332, doi: 10.1364/OE.15.005327 · Source: PubMed, 2007a.

Hu, Y., Vaughan, M., McClain, C., Behrenfeld, M., Maring, H., Anderson, D., Sun-Mack, S., Flittner, D., Huang, J. P., Wielicki, B., Minnis, P., Weimer, C., Trepte, C. and Kuehn, R.: Global statistics of liquid water content and effective number concentration of water clouds over ocean derived from combined CALIPSO and MODIS measurements, Atmos. Chem. Phys., 7, 3353–3359, doi:10.5194/acp-7-3353-2007, 2007b.

Hu, Y. X., Winker, D., Vaughan, M., Lin, B., Omar, A., Trepte, C., Flittner, D., Yang, P., Nasiri, S. L., Baum, B., Sun, W., Liu, Z. Y., Wang, Z. E., Young, S., Stamnes, K., Huang, J. P., Kuehn, R. and Holz, R.: CALIPSO/CALIOP Cloud Phase Discrimination Algorithm, J. Atmos. Ocean. Tech., 26, 2293–2309, doi: 10.1175/2009JTECHA1280.1, 2009.

Huang, J. P., Minnis, P., Lin, B., Wang, T. H., Yi, Y. H., Hu, Y. X., SunMack, S., and Ayers, K.: Possible influences of Asian dust aerosols on cloud properties and radiative forcing observed from MODIS and CERES, Geophys. Res. Lett., 33, L06824, doi: 10.1029/2005GL024724, 2006a.

Huang, J. P., Wang, Y. J., Wang, T. H., and Yi, Y. H,: Dusty cloud radiative forcing derived from satellite data for middle latitude regions of East Asia, Progress in Natural Science, 16, 1084-1089, doi: 10.1080/10020070612330114, 2006b.

Huang, J. P., Minnis, P., Lin, B., Wang, T. H., Yi, Y, H., Hu, Y. X., Sunmark, S., and Ayers, K.: Possible influences of Asian dust aerosols on cloud properties and radiative forcing observed from MODIS and CERES,Geophys. Res. Lett., 33, L06824, doi: 10.1029/2005GL024724, 2006c.

Huang, J. P., Ge, J. M., and Weng, F. Z.: Detection of Asia dust storms using multisensor satellite measurements, Remote Sens. Environ., 110, 186–191, doi: 10.1016/j.rse.2007.02.022, 2007.

Huang, J. P., Wang, T. H., Wang, W. C., Li, Z. Q., and Yan, H. R.: Climate effects of dust aerosols over East Asian arid and semi-arid regions, J. Geophys. Res., 119, 11398–11416, doi: 10.1002/2014JD021796, 2014.

Huang, J., Liu, J., Chen, B., and Nasiri, S. L.: Detection of anthropogenic dust using CALIPSO lidar measurements, Atmos. Chem. Phys., 15, 11653–11665, doi: 10.5194/acp-15-11653-2015, 2015.

Huang, Y. S., Dupont, L., Sarnthein, M., Hayes, J. M., and Eglinton, G.: Mapping of C4 plant input from North West Africa into North East Atlantic sediment, Geochimica Et CosmochimicaActa., 64(20), 3505-3513, doi: 10.1016/S0016-7037(00)00445-2, 2000.

Huang, J., Yu, H., Guan, X., Wang, G., and Guo, R.: Accelerated dryland expansion under climate change, Nature Clim. Change, doi: 10.1038/nclimate2837, 2015.

Jordan, N. S., Hoff, R. M., and Bacmeister, J. T.: Validation of Goddard Earth Observing System-version 5 MERRA planetary boundary layer heights using CALIPSO, J. Geophys. Res., 115, D24218, doi: 10.1029/2009JD013777, 2010.

Justice, C., Kendall, J., Dowty, P., and Scholes, R.: Satellite remote sensing of fires during the SAFARI campaign using NOAA ad- vanced very high resolution radiometer data, J. Geophys. Res., 101, 23851–23863, doi: 10.1029/95JD00623, 1996.

Kang, L.T., Huang J. P., and Chen, S. Y.: Long-term trends of dust events over Tibetan Plateau during 1961-2010. Atmo. Environ., 125(2016), 188-198, doi:10.1016/j.atmosenv.2015.10.085, 2015.

Kim, D., Chin, M., Bian, H., Tan, Q., Brown, M. E., Zheng, T., You, R., Diehl, T., Ginoux, P., and Kucsera, T.: The effect of the dynamic surface bareness on dust source function, emission, and distribution, J.G.R., 118,1-16, doi: 10.1029/2012JD017907, 2013.

Kim, D., Chin, M., Kemp, Eric, M., Tao, Z., Peters-Lidard, Chista, D., and Ginoux, P.: Development of high-resolution dynamic dust source function: A case study with a strong dust storm in a regional model, Atomos. Environ., 159, 11-25, doi:10.1016/j.atmosenv.2017.03.045, 2017.

Klein, G. K., Beusen, A., and Janssen, P.: Long term dynamic modeling of global population and built-up area in a spatially explicit way, HYDE 3.1. Holocene., 20(4): 565–573, doi: 10.1177/0959683609356587, 2010.

Klein, G. K., Beusen, A., Van Drecht, G., and DeVos, M.: The HYDE 3.1 spatially explicit database of human-induced global land-use change over the past 12,000 years, Global Ecol. Biogeogr., 20(1), 73-86, doi:10.1111/j.1466-8238.2010.00587.x, 2011.

Largeron, Y., Guichard, F., Bouniol, D., Couvreux, F., and Kergoat, L.: Can we use surface wind fields from meteorological reanalyses for Sahelian dust emission simulations? Geophys. Res. Lett., 42 (7), 2490-2499, doi:10.1002/2014GL062938, 2015.

Li, Z. Q., Lau, W. K.-M., Ramanathan, V., Wu, G., Ding, Y., Manoj, M. G., Liu, J., Qian, Y., Li, J., Zhou, T., Fan, J., Rosenfeld, D., Ming, Y., Wang, Y., Huang, J., Wang, B., Xu, X., Lee, S.-S., Cribb, M., Zhang, F., Yang, X., Zhao, C., Takemura, T., Wang, K., Xia, X., Yin, Y., Zhang, H., Guo, J., Zhai, P. M., Sugimoto, N., Babu, S. S., and Brasseur, G.

P.: Aerosol and monsoon climate interactions over Asia, Rev. Geophys., 54, doi:10.1002/2015RG000500, 2016.

Liu, C., Zhao, T. L., Yang, X. H., Liu, F., Han, Y. X., Luan, Z. P., He, Q., Mark, R., Yuen, W. K.: Observational study of formation mechanism, vertical structure, and dust emission of dust devils over the Taklimakan Desert, China , J. Geophys., 121(7), 3608-3618, doi:10.1002/2015JD024256, 2016.

Lo, C. P.: Modeling the population of China using DMSP Operational Line-scan System Nighttime Data. Photogramm. Eng. Remote Sens., 67, 1037-1047, 2001.

Luan, Z. P., Han, Y. X., Zhao, T. L., Liu, F., Liu , C.: Dust opacities inside the dust devil column in the Taklimakan Desert, Atmos. Meas. Tech., 10(1), 273-279, doi:10.5194/amt-2016-231, 2017.

Mahowald, M., and Luo, C.: A less dusty future? Geophys. Res. Lett., vol. 30, NO. 17, 1903, doi: 10.1029/2003GL017880, 2003.

Mahowald, N., Jickells, T. D., Baker, A. R., Artaxo, P., and Benitez-Nelson, C. R.: Global distribution of atmospheric phosphorus sources, concentrations and deposition rates, and anthropogenic impacts. Global Biogeochem. Cy., 22(4), 37-42, doi:10.1029/2008GB003240, 2008.

Marsham, J. H., P. Knippertz, N. S. Dixon, D. J. Parker, and G. M. S. Lister: The importance of the representation of deep convection for modeled dust-generating winds over West Africa during summer, Geophys. Res. Lett., 38, L16803, doi:10.1029/2011GL048368, 11.

Marticorena, B., Bergametti, G.: Modeling the atmospheric dust cycle: 1. Design of a soil-derived dust emission scheme, J. Geophys. Res. Atmos., 100 (D8) :16415–16430, doi:10.1029/95JD00690, 1995.

Meiyappan, P., and Jain, A. K.: Three distinct global estimates of historical land-cover change and land-use conversions for over 200 years, Front. Earth Sci., 6(2), 122-139, doi:10.1007/s11707-012-0314-2, 2012.

Meiyappan, P., Dalton, M., C. O'Neill, B., and Jain, A. K.: Spatial modeling of agricultural land use change at global scale, Ecological Modelling, 291, 152–174, doi: 10.1016/j.ecolmodel.2014.07.027, 2014.

Mitchell, D., Storey, D., Antonio, D., Tao, C., and Rosales-Kawasaki, L.: Urbanisation in Asia and the Pacific: Challenges for Responsible Land Administration and Land

Management. Scaling up Responsible Land Governance., 14-18, 2016.

Moulin, C., and Chiapello, I.: Impact of human-induced desertification on the intensification of Sahel dust emission and export over the last decades, Geophys.Res. Lett., 331 (18), 510-527, doi:10.1029/2006GL025923, 2006.

Munkhtsetseg, E., Shinoda, M., Ishizuka, M., Mikami, M., Kimura, R., and Nikolich, G.: A livestock trampling function for potential emission rate of wind-blown dust in a Mongolian temperate grassland, Atmos. Chem. Phys., 17, 11389-11401, doi:10.5194/acp-17-11389-2017, 2017.

O'Leary, M. H.: Carbon isotope fractionation in plants, Phytochem.,20, 553–568, 1981.

Penner, J. E., Charlson, R. J., Hales, J. M., Laulainen, N. S., Leifer, R., Novakov, T., Ogre, J., Radke, L. F., Schwartz, S. E., and Travis, L.: Quantifying and minimizing uncertainty of climate forcing by anthropogenic aerosols. Bull. Amer. Meteor. Soc., Vol. 75, No. 3, 380-400, 1994.

Redelsperger, J. L., Thorncroft, C. D., Diedhiou, A., Lebel, T., Parker, D. J., and Polcher, J.: African Monsoon Multidisciplinary Analysis: An International Research Project and Field Campaign, Bull. Amer. Meteor. Soc., 87 (12), 1739-1746, doi:10.1175/BAMS-87-12-1739, 2006.

Sage, R. F., and Monson, R. K.: C4 Plant Biology, Academic, San Diego, Calif., 1999.

Schefuβ, E., Rtmeyer, V., Stuut, JBW., Jansen, JHF., and Damesté, JSS.: Carbon isotope analyses of n-alkanes in dust from the lower atmosphere over the central eastern Atlantic, Geochim.Cosmochim.Ac., 67(10), 1757-1767, doi:10.1016/S0016-7037(02)01414-X, 2003.

Scott., P.R., Sudmeyer., R.A.: Evapotranspiration from agricultural plant communities in the high rainfall zone of the southwest of Western Australia, Journal of Hydrology., 146 (1-4) :301-319, doi:10.1016/0022-1694(93)90281-D, 1993.

Semborski, R. J.: Dust from Anthropogenic Sources in the Snowpack on Glaciers in the Cordillera Blanca, Peru, Agu Fall Meeting, 2013.

Shao, Y. P.: Simplification of a dust emission scheme and comparison with data. J. Geophys. Res., 109, D10202, doi: 10.1029/2003JD004372, 2004.

Shao, Y. P., and Dong, C. H.: A review on East Asian dust storm climate, modelling and monitoring, Global Planet.Change, 52, 1-22, doi:10.1016/j.gloplacha.2006.02.011, 2006.

Shao, Y.P, Wyrwoll, K. H., Chappell,A.: Dust cycle: An emerging core theme in Earth system science, Aeolian Res., 2, 181-204, doi:10.1016/j.aeolia.2011.02.001, 2011.

Shi, A.: The impact of population pressure on global carbon dioxide emissions, 1975 - 1996: evidence from pooled cross-country data, Ecological Economics., 44 (1) :29-42, doi:10.1016/S0921-8009(02)00223-9, 2003.

Sokolik, I. N., and Toon, O. B.: Direct radiative forcing by airborne mineral aerosols, J. Aerosol Sci., 27 (6584), 11-12(2), doi:10.1016/0021-8502(96)00078-X, 1996.

Soulé, P.T., and Dehart, J.L.: Assessing IPAT Using Production- and Consumption-based Measures of I, Social Science Quarterly., 79 (4) :754-765, 1998.

Sutton, P.: Modeling population density with nighttime satellite imagery and GIS, Computers, Environment and Urban Systems., 21(3-4), 227-244, 10.1016/S0198-9715(97)01005-3 , 1997.

Tegen, I., and Fung, I.: Modeling of mineral dust in the atmosphere: Sources, transport, and optical thickness, J. Geophys. Res., 99 (D11) :22897–22914, doi:10.1029/94JD01928 , 1994

Tegen, I., and Fung, I.: Contribution to the atmospheric mineral aerosol load from land surface modification. J. Geophys. Res., 18,707-18,726, doi:10.1029/95JD02051, 1995.

Tegen, I., Werner, M., Harrison, S.P, and Kohfeld, K.E.: Relative importance of climate and land use in determining present and future global soil dust emission, Geophysical Research Letters, 31 (5) :325-341, doi:10.1029/2004GL021560, 2004.

Wang, Z.; Zhang, H.; Li, J.; Jing, X.; Lu, P.: Radiative forcing and climate response due to the presence of black carbon in cloud droplets. J. Geophys. Res. Atmos., 118, 3662-3675, doi: 10.1002/jgrd.50312, 2013.

Wang, Z. L., Zhang, H., Shen, X. S.: Radiative forcing and climate response due to black carbon in snow and ice, Adv. Atmos. Sci., 28, 1336-1344, doi: 10.1007/s00376-011-0117-5, 2012.

Winker, D. M., Hunt, W. H., and McGill, M. J.: Initial performance assessment of CALIOP, Geophys. Res. Lett., 34, L19803, doi:10.1029/2007GL030135, 2007.

Xi, X., and Sokolik, I. N.: Seasonal dynamics of threshold friction velocity and dust emission in Central Asia, J. Geophys. Res. Atmos., 120 (4) :1536-1564, doi:10.1002/2014JD022471, 2015.

Xi, X., and Sokolik, I. N.: Quantifying the anthropogenic dust emission from agricultural land use and desiccation of the Aral Sea in Central Asia, J. Geophys. Res. Atmos., 121(20), doi:10.1002/2016JD025556, 2016.

Atmos. Chem. Phys. Discuss., https://doi.org/10.5194/acp-2017-890
Manuscript under review for journal Atmos. Chem. Phys.
Discussion started: 1 December 2017


Atmospheric Chemistry and Physics
Open Access
EGU
Discussions

Ye, H., Zhang, R., Shi, J., Huang, J., Warren, G. S., and Fu, Q.: Black carbon in seasonal snow across northern Xinjiang in northwestern China, Environ. Res. Lett., 7, 044002, doi:10.1088/1748-9326/7/4/044002, doi:10.1088/1748-9326/7/4/044002, 2012.

York, R., Rosa, E.A., and Dietz, T.: STIRPAT, IPAT and ImPACT: analytic tools for unpacking the driving forces of environmental impacts, Ecological Economic, 46 (3) :351-365, doi:10.1016/S0921-8009(03)00188-5, 2003.

Yu, H., Remer, L. A., Chin, M., Bian, H., Tan, Q., Yuan, T., and Zhang, Y.: Aerosols from overseas rival domes- tic emissions over North America, Science, 337, 566–569, doi:10.1126/science.1217576, 2012.

Zender, C. S., Bian, H., and Newman, D.: Mineral Dust Entrainment and Deposition (DEAD) model: Description and 1990s dust climatology, J. Geophys.Res. Atmos., 108(D14), 10—1029, doi: 10.1029/2002JD002775, 2003.

Zender, C. S., Miller, R.,and Tegen,I.:Quantifying mineral dust mass budgets: Terminology, constraints, and current estimates., Eos.Trans. AGU, 85(48), 509–512, doi:10.1029/2004EO480002, 2004.

Zender, C. S., and Kwon, E.Y. :Regional contrasts in dust emission responses to climate, J. Geophys.Res. Atmos., 110 (D13) :1665-1677, doi:10.1029/2004JD005501, 2005.

Zhao, C., Liu, X., Leung, L. R., and Johnson, B.: The spatial distribution of mineral dust and its shortwave radiative forcing over North Africa: Modeling sensitivities to dust emissions and aerosol size treatments. Atmos.Chem. Phys., 10, 8821–8838, doi:10.5194/acp-10-8821-2010, 2010.

Zhuo, L., Shi, P.J., Chen, J., and Ichinose, T.: Application of compounded night light index derived from DMSP/OLS data to urbanization analysis in China in the 1990s, Acta. Geogr. Sin., 58, 893–902, doi:10.11821/xb200306013, 2003. (In Chinese)

Zhao C., Chen, S., Leung, L.R., Qian, Y., Kok, J.F., Zaveri, R.A., and Huang, J.: Uncertainty in Modeling Dust Mass Balance and Radiative Forcing from Size Parameterization, Atmos. Chem. Phys., 13(21), 10733-10753, doi:10.5194/acp-13-10733-201, 2013.

Zhang, H., Wang, Z. L., Guo, P. W., and Wang, Z. Z.: A modeling study of the effects of direct radiative forcing due to carbonaceous aerosol on the climate in East Asia, Adv. Atmos. Sci., 26(1), 1-10, doi: 10.1007/s00376-009-0057-5, 2009a.

Zhang, H., and Wang, Z. L.: Advances in Studies of Black Carbon Effects on Climate, Adv. Climate Change Res., 5, 311-317, doi: 10.3969/j.issn.1673-1719.2009.06.001, 2009b. (In Chinese)

Zhang, H., Wu, J.-X.: A study of radiative forcing and global warming potentials due to HFCs, Am. Institute Phys., doi: 10.1063/1.3117056, 2008.

Zhang, Z.G., Shao., Y.S., and Xu., Z.X.: Prediction of urban water demand on the basis of Engel's coefficient and Hoffmann index: case studies in Beijing and Jinan, China, Water Sci. Technol., 62(2), 410-418, doi:10.2166/wst.2010.290, 2010.

Zheng, Y., Zhao, T. L., Che, H. Z., Liu, Y., Han, Y. X., Liu, C., Xiong, J., Liu, J. H., and Zhou, Y. K., A20-year simulated climatology of global dust aerosol deposition, Sci. Total Environ., 557, 861-868, doi:10.1016/j.scitotenv.2016.03.086, 2016.

Atmos. Chem. Phys. Discuss., https://doi.org/10.5194/acp-2017-890
Manuscript under review for journal Atmos. Chem. Phys.
Discussion started: 1 December 2017


Table 1. Summary of estimated anthropogenic dust fractions in previous studies

| Research | Resolution | Region | Time period | Fraction |
|---|---|---|---|---|
| Tegen and Fung, 1995 | 8° x 10° | Global | -- | 30–50% |
| Mahowald and Luo, 2003 | 1.9° x 1.9° | Global | 1980–2099 | 14–60% |
| Tegen et al., 2004 | 3.75° x 5° | Global | 1983–1992 | <10% |
| Huang et al., 2015 | -- | Global | 2007–2010 | 25% |

Atmos. Chem. Phys. Discuss., https://doi.org/10.5194/acp-2017-890
Manuscript under review for journal Atmos. Chem. Phys.
Discussion started: 1 December 2017


Table 2. Land cover classifications

| | |
|---|---|
| 1 | Tropical Evergreen Broadleaf Forest |
| 2 | Tropical Deciduous Broadleaf Forest |
| 3 | Temperate Evergreen Broadleaf Forest |
| 4 | Temperate Evergreen Needleleaf Forest |
| 5 | Temperate Deciduous Broadleaf Forest |
| 6 | Boreal Evergreen Needleleaf Forest |
| 7 | Boreal Deciduous Needleleaf Forest |
| 8 | Savanna |
| 9 | $C_3$ Grassland/Steppe |
| 10 | $C_4$ Grassland/Steppe |
| 11 | Dense Shrubland |
| 12 | Open Shrubland |
| 13 | Tundra |
| 14 | Desert |
| 15 | Polar-Desert/ Rock/ Ice |
| 16* | Secondary Tropical Evergreen Broadleaf Forest |
| 17* | Secondary Tropical Deciduous Broadleaf Forest |
| 18* | Secondary Temperate Evergreen Broadleaf Forest |
| 19* | Secondary Temperate Evergreen Needleleaf Forest |
| 20* | Secondary Temperate Deciduous Broadleaf Forest |
| 21* | Secondary Boreal Evergreen Needleleaf Forest |
| 22* | Secondary Boreal Deciduous Needleleaf Forest |
| 23* | Water/Rivers |
| 24* | $C_3$ Cropland |
| 25* | $C_4$ Cropland |
| 26* | $C_3$ Pastureland |
| 27* | $C_4$ Pastureland |
| 28* | Urban land |

*Types of anthropogenic land cover

Atmos. Chem. Phys. Discuss., https://doi.org/10.5194/acp-2017-890
Manuscript under review for journal Atmos. Chem. Phys.
Discussion started: 1 December 2017

Atmospheric Chemistry and Physics
Open Access
Discussions

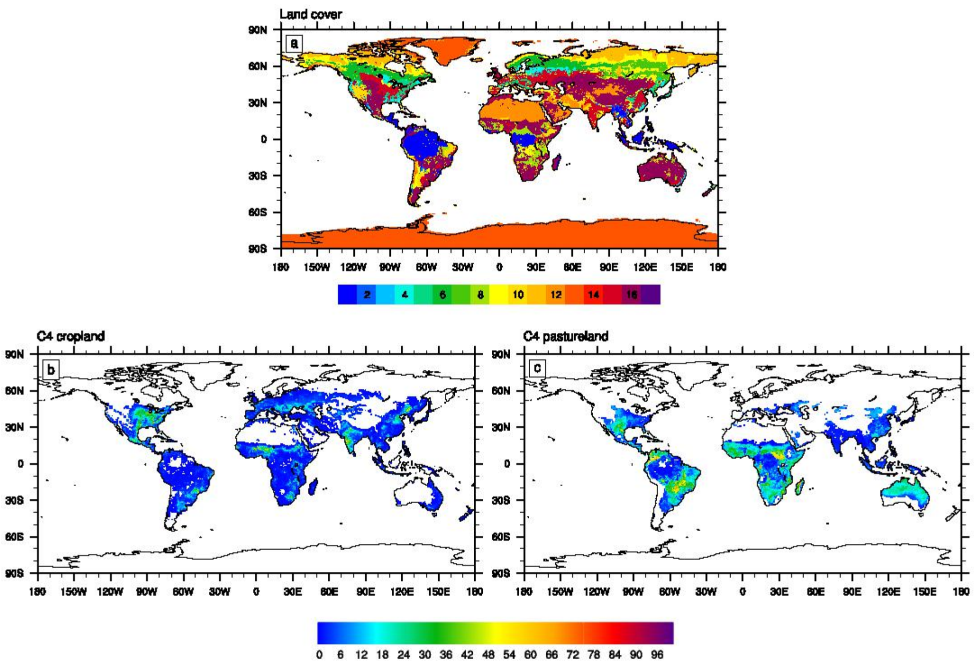


Figure 1. Spatial distribution of land cover from Meiyappan and Jain (2012) and the percentages of $C_4$ croplands and $C_4$ pasturelands from 2007 to 2010.

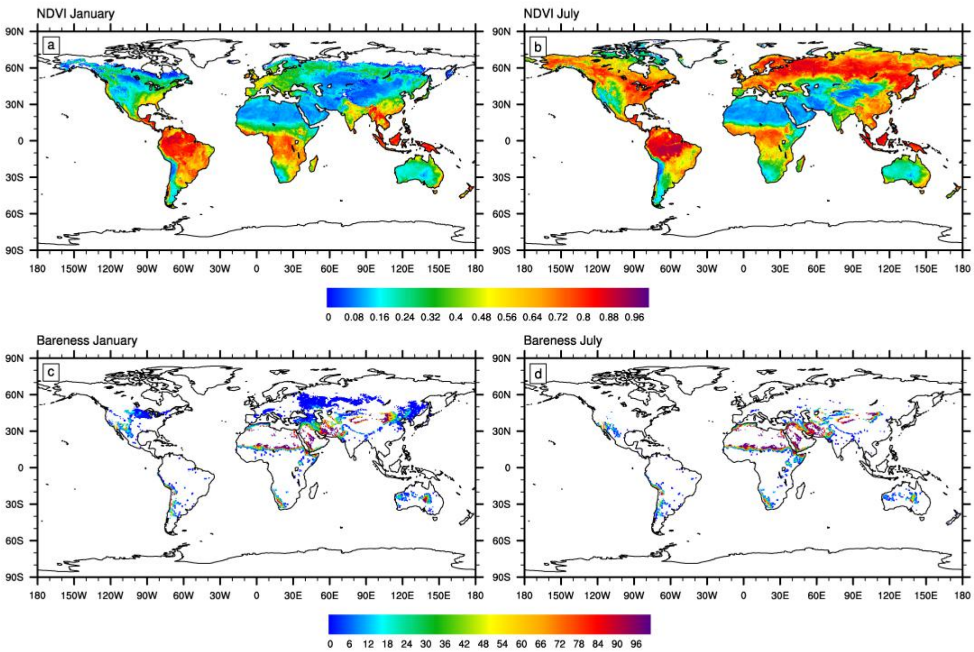


Figure 2. Spatial distribution of normalized difference vegetation index (NDVI) and surface bareness (%) in January (a, c) and July (b, d), respectively, from 2007 to 2010.

Atmos. Chem. Phys. Discuss., https://doi.org/10.5194/acp-2017-890
Manuscript under review for journal Atmos. Chem. Phys.
Discussion started: 1 December 2017


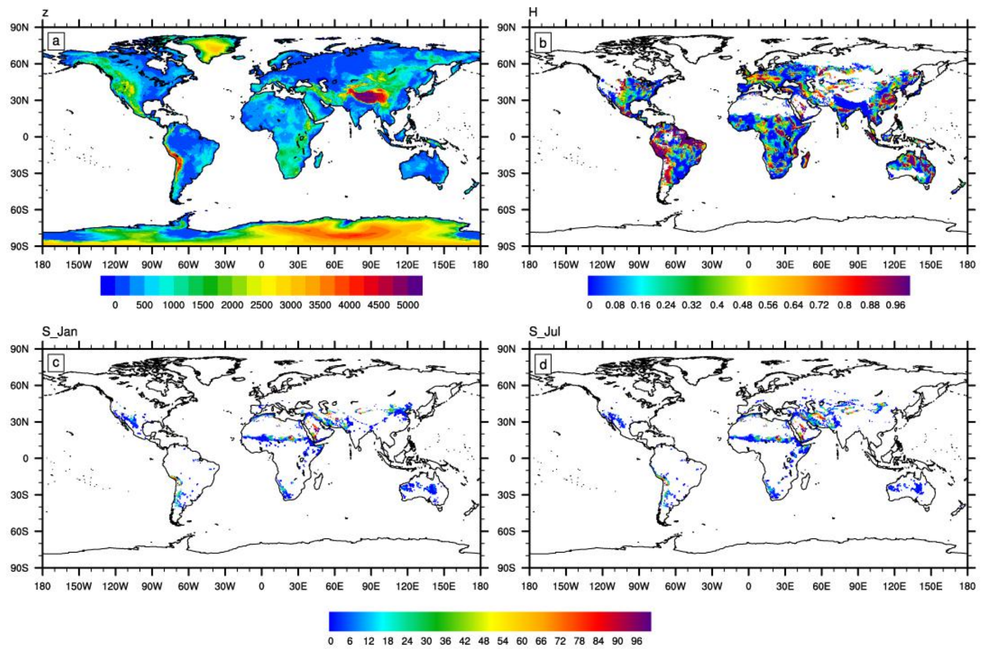


Figure 3. Spatial distribution of global altitude z (a, unit: m), the topographical depression H (b, unit: dimensionless), and the dynamic dust source function Sad (%) in January (c) and July (d), respectively.

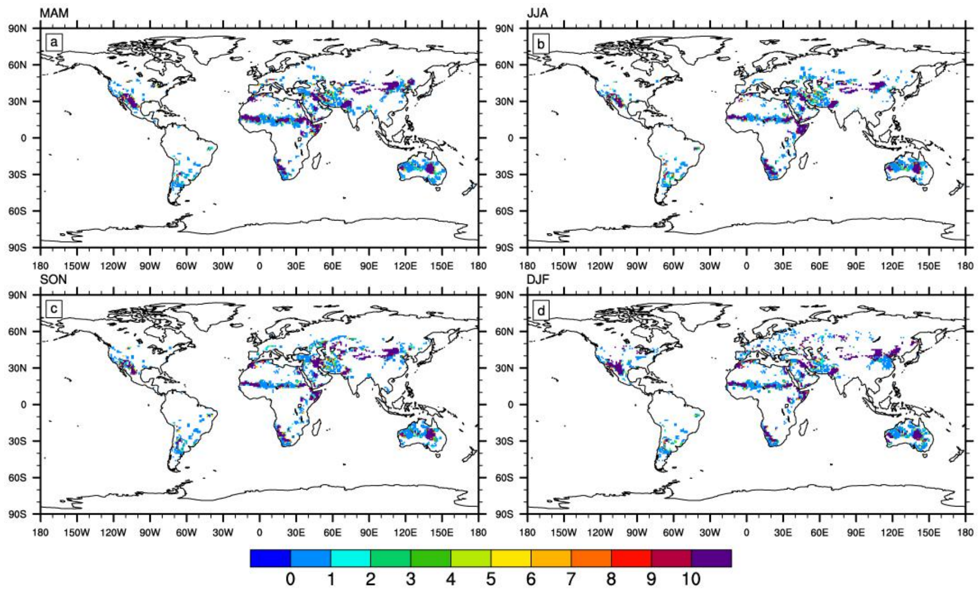


Figure 4. Seasonal variations of simulated indirect anthropogenic dust flux (μg $m^{-2}$ $s^{-1}$) from 2007 to 2010.

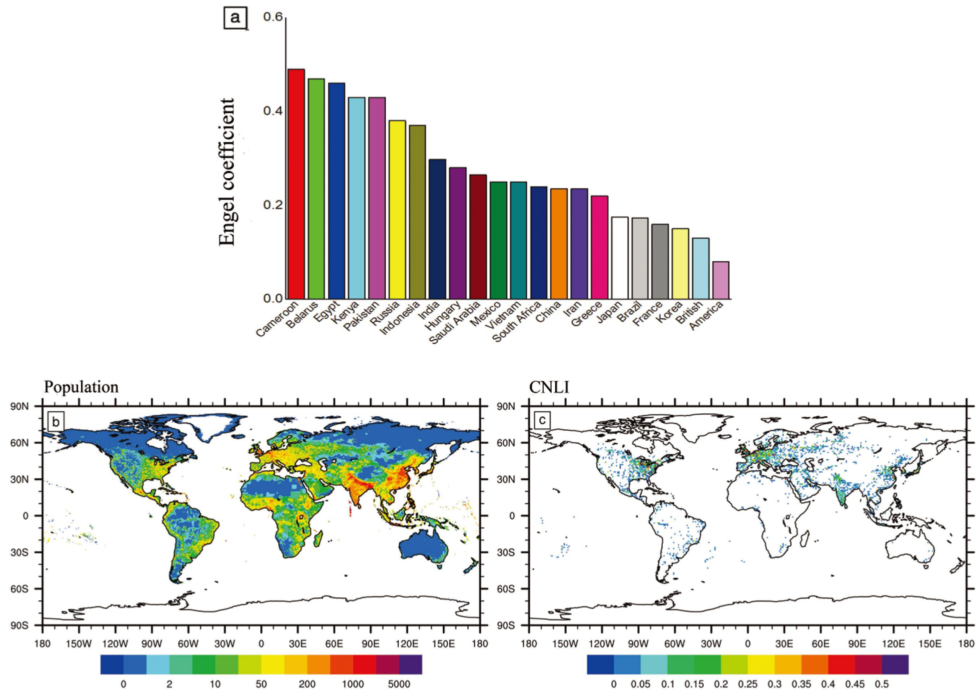


Figure 5. Engel coefficients in 21 countries (a), population density (b, unit: persons km$^{-2}$), and compounded nighttime light index (CNLI) (c) at global scale from 2007 to 2010.

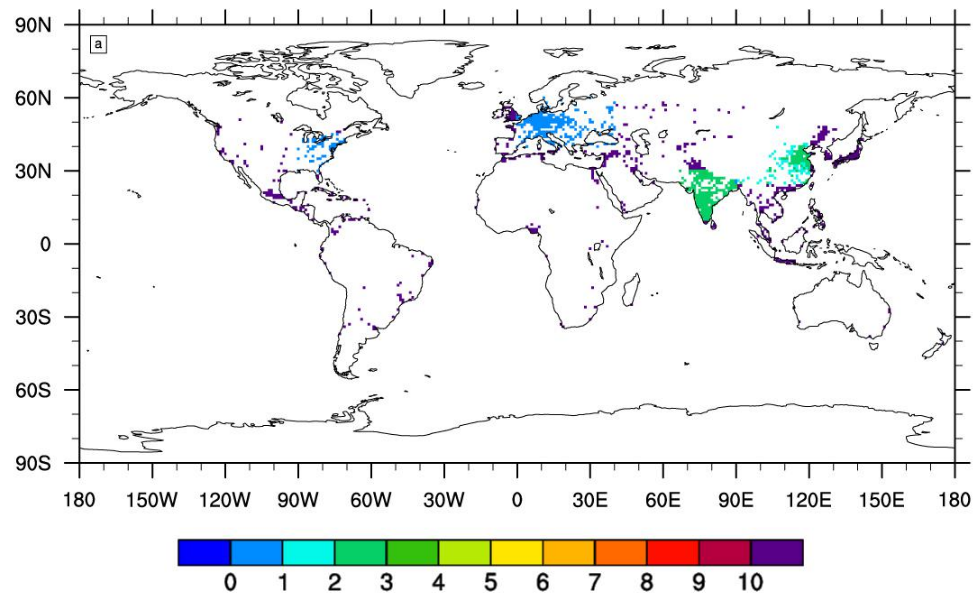


Figure 6. Spatial distributions of simulated direct anthropogenic dust flux (μg $m^{-2}$ $s^{-1}$) from 2007 to 2010.

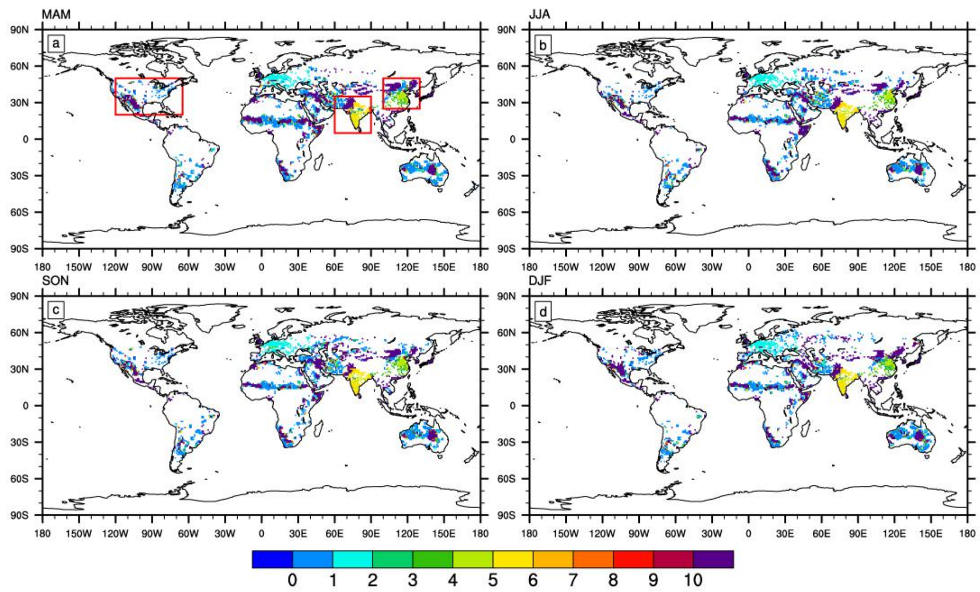


Figure 7. Seasonal variations in simulated anthropogenic dust flux (μg $m^{-2}$ $s^{-1}$) from 2007 to 2010. The red boxes represent regions prone to anthropogenic dust emissions and were used for further analysis.

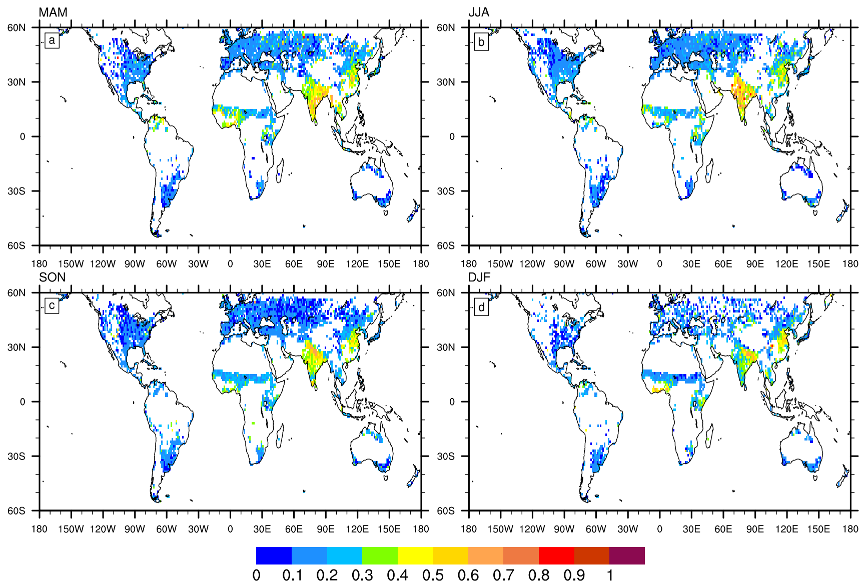


Figure 8. Seasonal variations in the anthropogenic dust column (g m$^{-2}$) based on CALIPSO retrievals from 2007 to 2010.

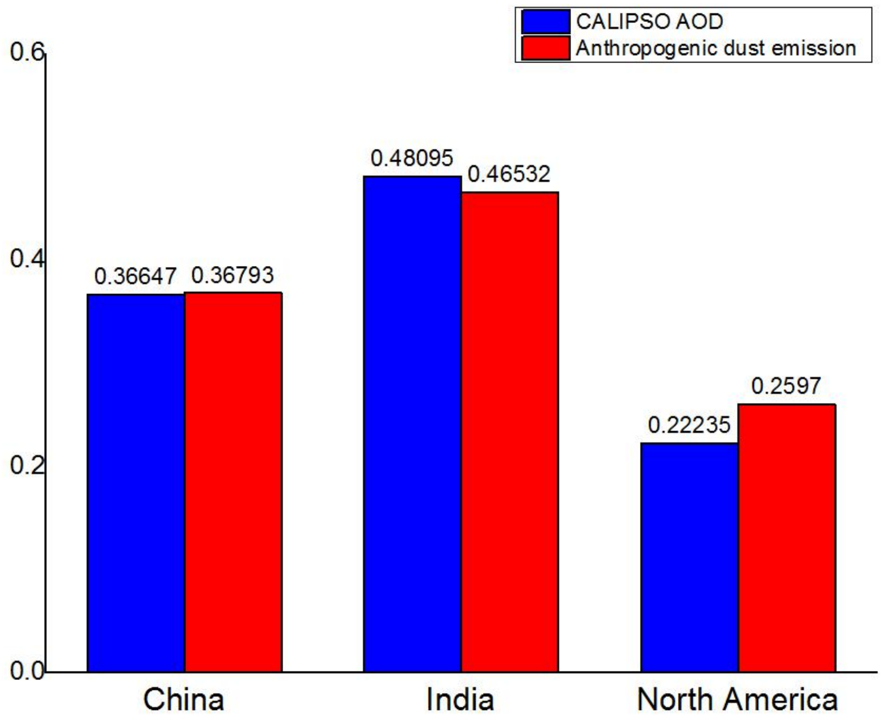


Figure 9. Normalizations of anthropogenic dust from CALIPSO retrievals and simulations in China, India, and North America.

Atmos. Chem. Phys. Discuss., https://doi.org/10.5194/acp-2017-890
Manuscript under review for journal Atmos. Chem. Phys.
Discussion started: 1 December 2017

Atmospheric Chemistry and Physics Discussions

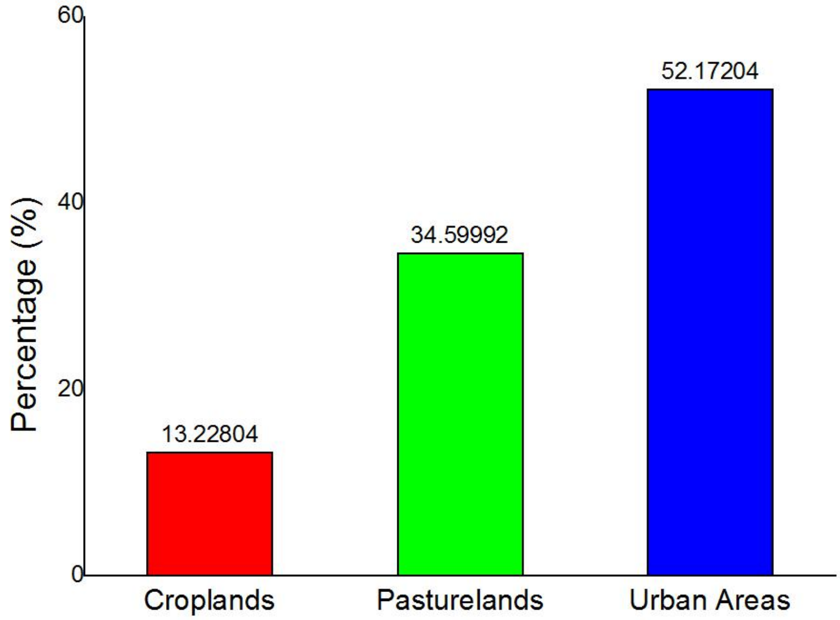


Figure 10. Percentages of anthropogenic dust emission flux in croplands, pasturelands, and urban areas.

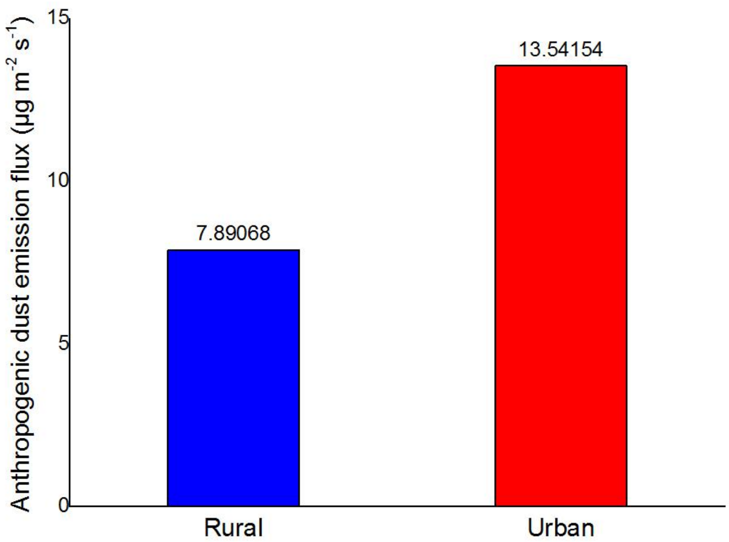


Figure 11. Average anthropogenic dust emission flux (μg $m^{-2}$ $s^{-1}$) in urban and rural areas from 2007 to 2010.